Chapter 4 : Lithium Tests

From Chapter 3 it is evident that lithium is an important constituent of the corrosion products formed when stainless steel is immersed in a molten alkali salt. This was also seen by Frangini et al. [1] who grow protective perovskite coatings over a $LiFeO_2$ layer on stainless steel 316L in a molten carbonate melt [1]. Therefore, further tests were run to determine the role lithium plays in corrosion of stainless steel 316L.

Two tests were run simultaneously using a binary and a ternary eutectic salt, and Table 4.1 gives information on the eutectic mixtures used.

Table 4.1: Information about the two eutectic mixtures utilised in this chapter [2, 3].

	Binary	**Ternary**
Compounds present	Potassium chloride (KCl) Sodium chloride (NaCl)	Potassium chloride (KCl) Sodium chloride (NaCl) Lithium chloride (LiCl)
Eutectic composition	50 mol. %: 50 mol. % 56.06 wt. %: 43.94 wt. %	36.09 mol. %: 8.27 mol. %: 55.64 mol. % 48.63 wt.%: 8.74 wt. %: 42.63 wt. %
Eutectic temperature	652°C	429°C

These experiments required a higher temperature than the experiments run in Chapter 3 due to the higher eutectic temperature of the binary salt. Initially, tests were run to determine the melting temperature of the binary salt. The two separate salts were thoroughly mixed and heated, and the approximate melting point, 750°C, was found to be less than the melting temperature of both constituent compounds, which can be found in Table 2.3. Week-long tests were run at 750°C, and also heating the salt up to 750°C to melt it and cooling to 700°C. No differences were seen, therefore the sample was heated to 750°C and subsequently cooled to 700°C.

Two crucibles, containing a binary and ternary eutectic, with coupons of stainless steel 316L, were pre-heated to 120°C to evaporate water, then further heated to 750°C, cooled to 700°C, and left for a predetermined length of time (one, three and four weeks). As observed in Chapter 3, the initial three week tests showed a different result, therefore they were repeated. It is striking once again that it is

the three-week test that showed an inconsistent result compared to the other time points, when these tests were run entirely independently of the work described in Chapter 3.

The results of these experiments are shown in Figure 4.1.
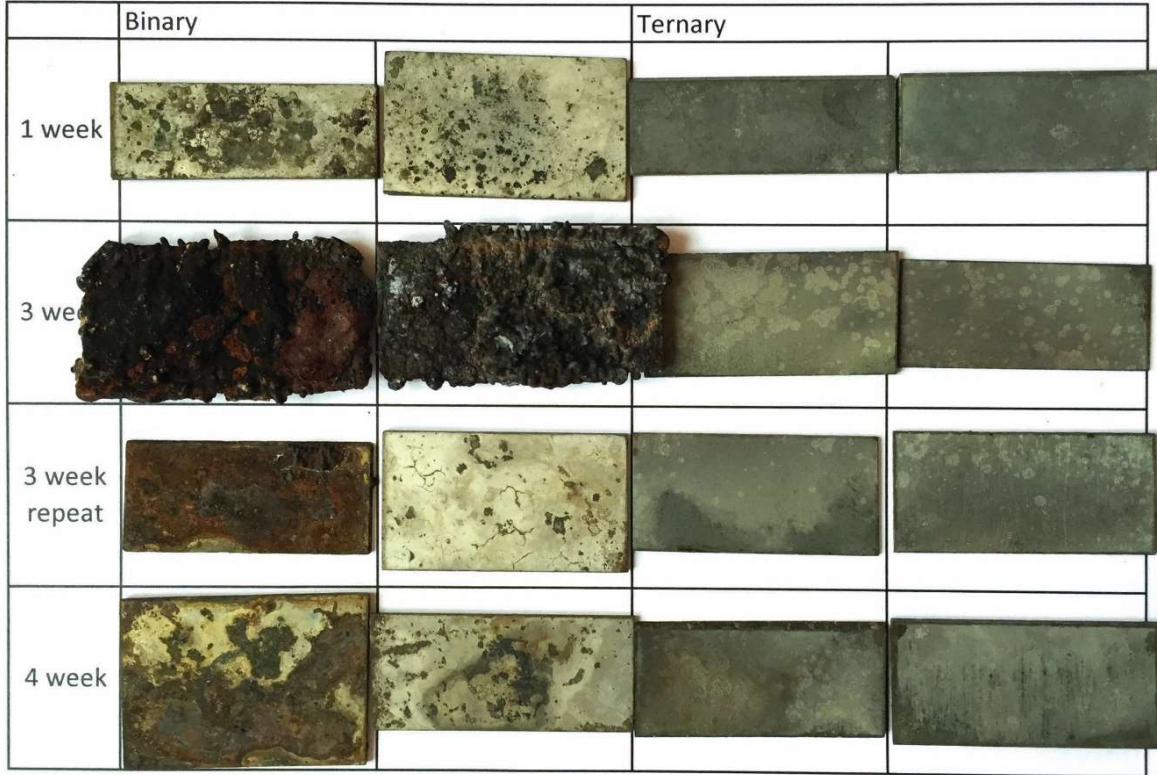
Figure 4.1: The ternary and binary test results (from top to bottom: 1 week, 3 week, 3 week (repeat) and 4 week).

When the one, four, and repeated three week tests are analysed they follow a similar pattern; the binary tests show a green/brown corrosion product, with increasing surface coverage as immersion time increases, this eventually becomes a brown corrosion layer that readily spalls. The initial three week tests show the formation of a highly textured brown/black corrosion layer which covers the entire surface and does not follow the pattern observed for the other samples. This appears similar to the results obtained in the three week stainless steel 316L tests but with full coverage, and is similar to the results obtained by Sellers et al [4] where molten FLiNaK leaked at 850°C and it was believed that K_2NaCrF_6 formed [4]. The ternary results are all consistent, showing the formation of a grey corrosion layer over the entire surface of the stainless steel 316L; this was also seen in Chapter 3, when the three week results are omitted.

The formation of spinels in a molten salt has been reported by Cho et al. and by Hiramatsu et al. [5, 6]. From the visual analysis, it can be concluded that lithium aids in the formation of a uniform protective layer over the coupon.

The mass change for each of the samples is shown Figure 4.2, where it should be noted that the weight change of the specimen is due to loss of initial material and formation of corrosion products.
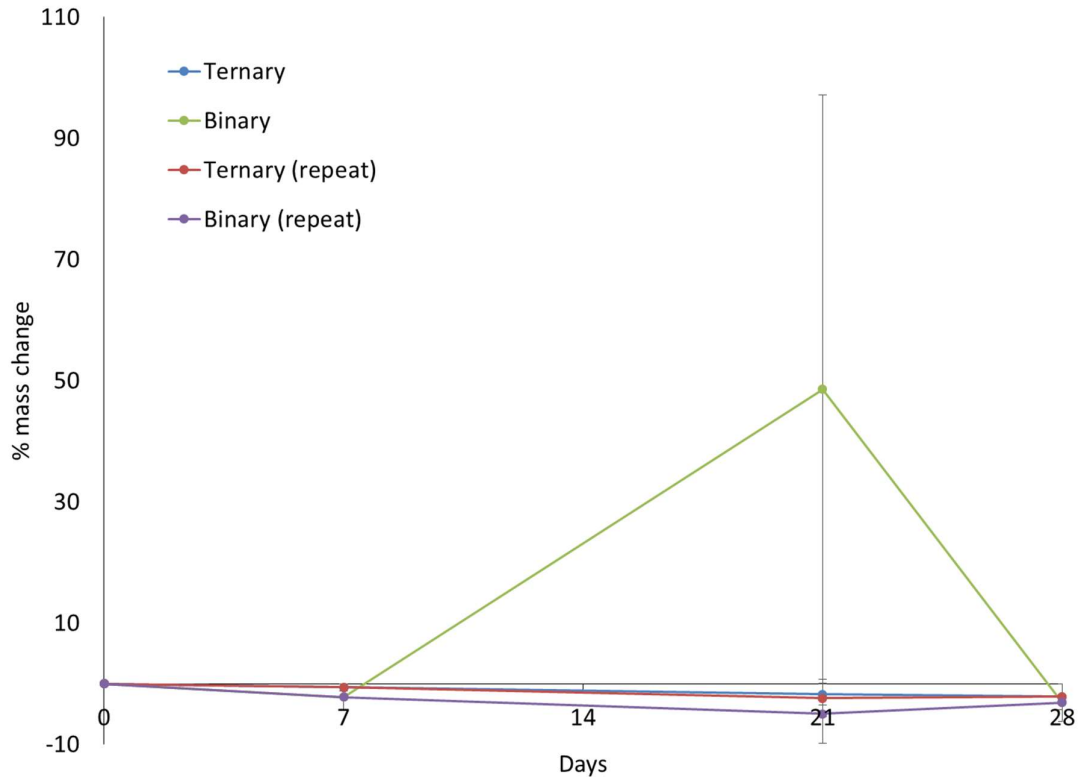
Figure 4.2: Mass loss of stainless steel 316L samples during corrosion testing, as a percentage of initial coupon mass.

Figure 4.2 shows a small percentage mass loss in the ternary eutectic salt, and as immersion time increases the mass loss increases. This is similar to the results seen in Chapter 3 (Figure 3.9) and is not surprising as the same experiment is taking place but at a higher temperature. The binary results show similar trends, with the gradual loss of material as immersion time increases, but both the initial and repeat three week binary tests show unusual results. The initial three week test shows an enormous mass increase and although this result alone is surprising, if analysed in conjunction with Figure 4.1 this large mass increase is clearly due to the thick layer that has formed on the sample. The results obtained for the repeated three week test run in a binary molten chloride salt show a slightly larger mass decrease compared to the four week test, but when the error associated with these measurements is accounted for the difference is negligible.

4.1: XRD

Figure 4.3 shows the diffraction patterns for the ternary experiments. Each of the ternary diffraction patterns show a peak at 18° 2θ this is attributed to the formation of a lithium spinel within the sample. It is possible to see relatively consistent peaks throughout the ternary samples at approximately 36,

37, 44, 46, 51, 58, 64, 65 and 67° 2θ. Some of these can be identified as stainless steel (44 and 51°), with the slight peak shift attributed to the loss of chromium and possibly iron from the stainless steel. The three week repeat test also shows the presence of peaks at approximately 27 and 32° 2θ, attributed to potassium chloride.

The ternary results are similar to results obtained in Chapter 3, whereby a spinel, believed to be lithium chromium oxide, is present. As previously mentioned, it is difficult to determine which metal is present as the diffraction patterns of different lithium spinel phases are very similar (Figure 3.4) and as the diffraction patterns for the tested samples do show a small amount of noise, pinpointing the exact composition of the phase via XRD is difficult.
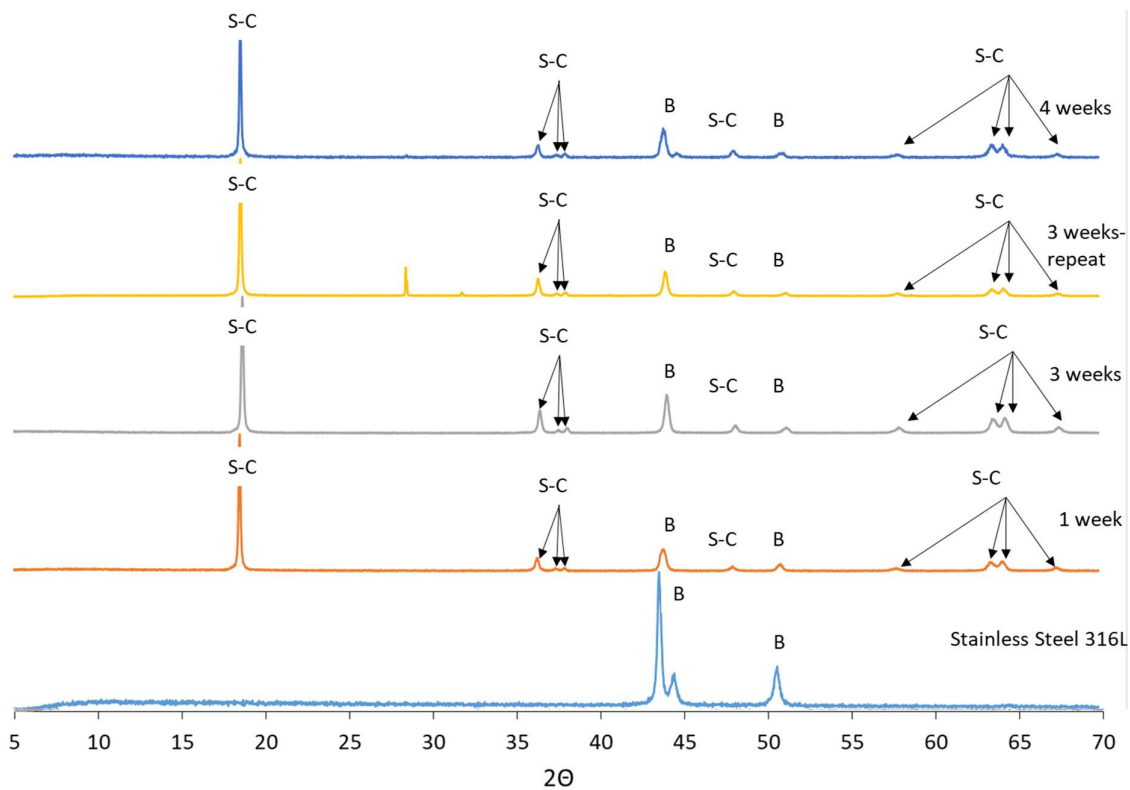
Figure 4.3: X-ray diffraction patterns for the stainless steel 316L samples immersed in a ternary eutectic alkali salt. S-C indicates LiCrO₂ spinel, and B is the bulk steel.

The binary tests, shown in Figure 4.4, show more disordered diffraction patterns than those obtained for the ternary tests. This is expected as a uniform crystalline product is not forming on the surface as was observed in the ternary samples. Peaks corresponding to the stainless steel can be observed at approximately 44 and 51° 2θ in the 1 week, 3 week repeat and four week tests, and the small peak shift observed is attributed to the loss of chromium and possibly iron from within the stainless steel bulk. Peaks that correspond to the corrosion product have low intensity as the corrosion product does not cover the whole sample, but can be seen at approximately 24, 34, 35, 42 and 46° 2θ. The data set

collected for the three week test is extremely noisy and attempts at obtaining results to further define the peaks have been unsuccessful.

The one week binary test shows the presence of iron oxide along with chromium oxide, iron chloride and salt, the salt is likely to be present due to ineffecient packing of the corrosion product allowing it to become trapped. The binary three week test results are extremely noisy and therefore results from this are not going to be reliable. The three week test was then repeated, and the XRD pattern suggests similar results to those previously observed: chromium oxide and iron oxide are present in the sample, and this is similar for the four week test.
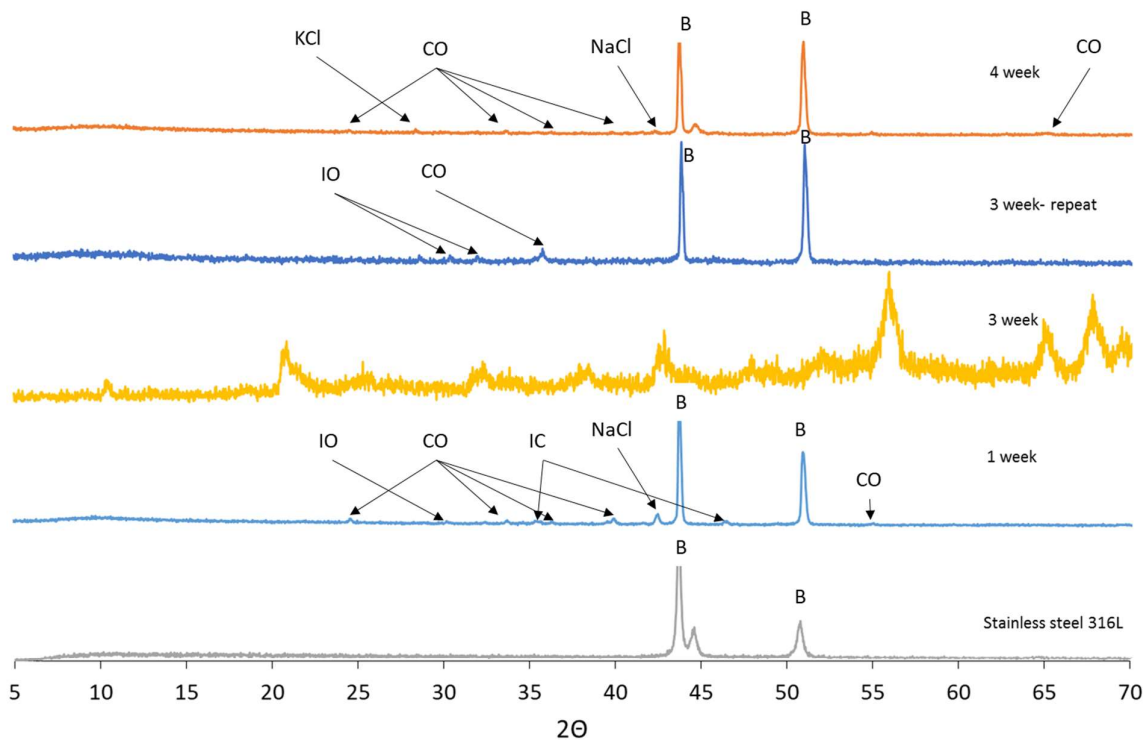
Figure 4.4: X-ray diffraction patterns for the stainless steel 316L samples immersed in a binary eutectic alkali salt. Here CO is Cr$_2$O$_3$, IO is Fe$_2$O$_3$, B is the bulk steel, and NaCl and KCl represent each of the salts. It should be noted that the diffraction patterns have been scaled and therefore it is only possible to identify phases, not to quantitatively compare intensities to one another.

The XRD pattern confirms that a lithium-containing product is formed in the ternary tests, but the exact compound is difficult to classify as the XRD patterns for lithium metal oxides (shown in Figure 3.4) are all very similar, but from previous results it is highly likely that lithium chromium oxide has formed.

The XRD data suggest that metal oxides are being formed on the surface of the samples immersed in the binary eutectic. As expected, the peak corresponding to lithium is not present. Chromium oxide

and iron oxide appear in the XRD patterns (excluding the three week test, which is too noisy to confirm the presence of any particular product).

4.2 Surface SEM

4.2.1: Ternary Results

The BSE results obtained for the samples immersed in the ternary salt (Figure 4.5) are similar to previous results in Chapter 3, where a smooth corrosion layer has formed over the majority of the surface of all the samples. Surface coverage has increased as immersion time increases; this is to be expected as the coupon is immersed in the molten chloride for longer, allowing the elements to leach out of the bulk (marked as 2 on the one week image) and form the corrosion layer (marked as 1). The repeated three week test shows a slightly higher surface coverage compared to week one, and the corrosion layer is thicker along the grain boundaries. As the sample has been immersed for a longer period of time grain boundary attack will be more prominent, as elements within the steel (usually chromium, a major element within the corrosion product) migrate to the grain boundaries [7]. Furthermore, the three and four week samples appear to show another product on the surface of the sample (marked as 3). The depth perception of these images is difficult to quantify, but it does not appear to be the bulk surface and will be investigated further via EDX and cross sectional analysis. The results for the two three week tests are comparable to the results obtained in Chapter 3, where two samples in seemingly the exact same environment give two different results.

It appears that the initial ternary three week test has caused heavier corrosion compared to the repeated test. It can therefore be concluded that the level of corrosion relies on both the presence of lithium and the immersion time, which Shankar and Mudali state can cause morphological changes [8].
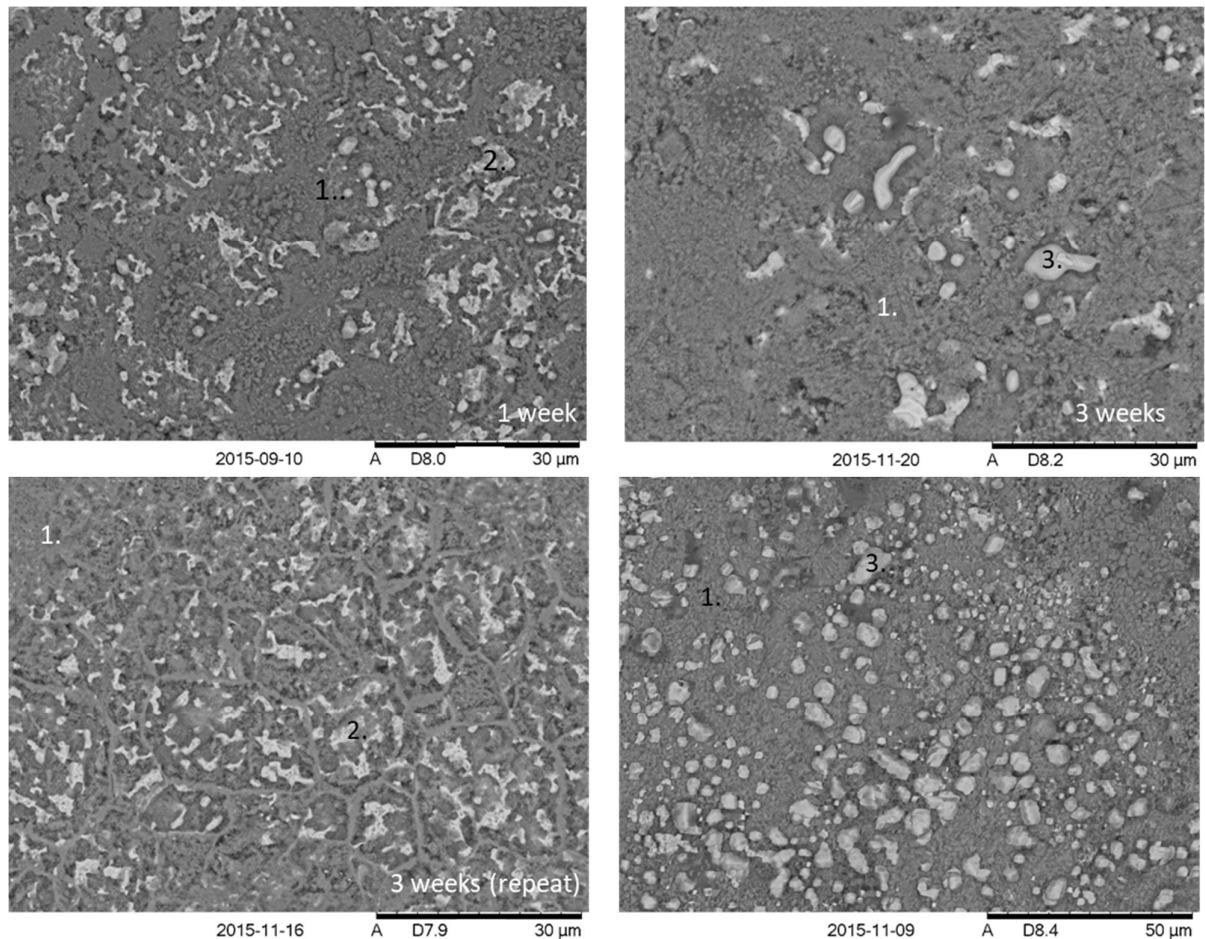
Figure 4.5: BSE Images of stainless steel 316L held in a ternary molten alkali chloride bath for a predetermined length of time (stated at the bottom of each image).

The EDX data for the four week test are shown in Figure 4.6, and it is clear that chromium and oxygen make up corrosion product 1. This is seen throughout Chapter 3 and also in the literature by Shankar and Mudali, and by Olson et al. [8, 9]. The presence of chromium within the corrosion product is expected as chromium sensitisation, whereby chromium migrates to grain boundaries, occurs between 723 K-1123 K (450°C – 850°C) [10].

There appears to be enhanced corrosion on the initial three week test and four week test samples, forming corrosion product 3. The further corrosion product 3 appears to contain iron, but it is difficult to say which anion, if any is present, and further insight will be sought during cross sectional SEM/EDX as presented below. Along with the presence of iron, there appears to be a much thicker chromium oxide corrosion layer on the initial three week and four week tests, when compared to the one week and repeated three week tests where the bulk 2 can still be seen and there is no indication that an iron compound has formed.

The transformation of a corrosion product after prolonged immersion was reported by Biedenkopf [11], whereby after 1000 hours the $LiFe_5O_8$ present at 500 hours completely transformed into $LiFeO_2$ [11]. This could also explain the 'anomalous result' obtained in the initial three week stainless steel 316L tests in Chapter 3, as it is possible that due to the prolonged immersion time an iron compound has formed in the initial three week and four week tests.
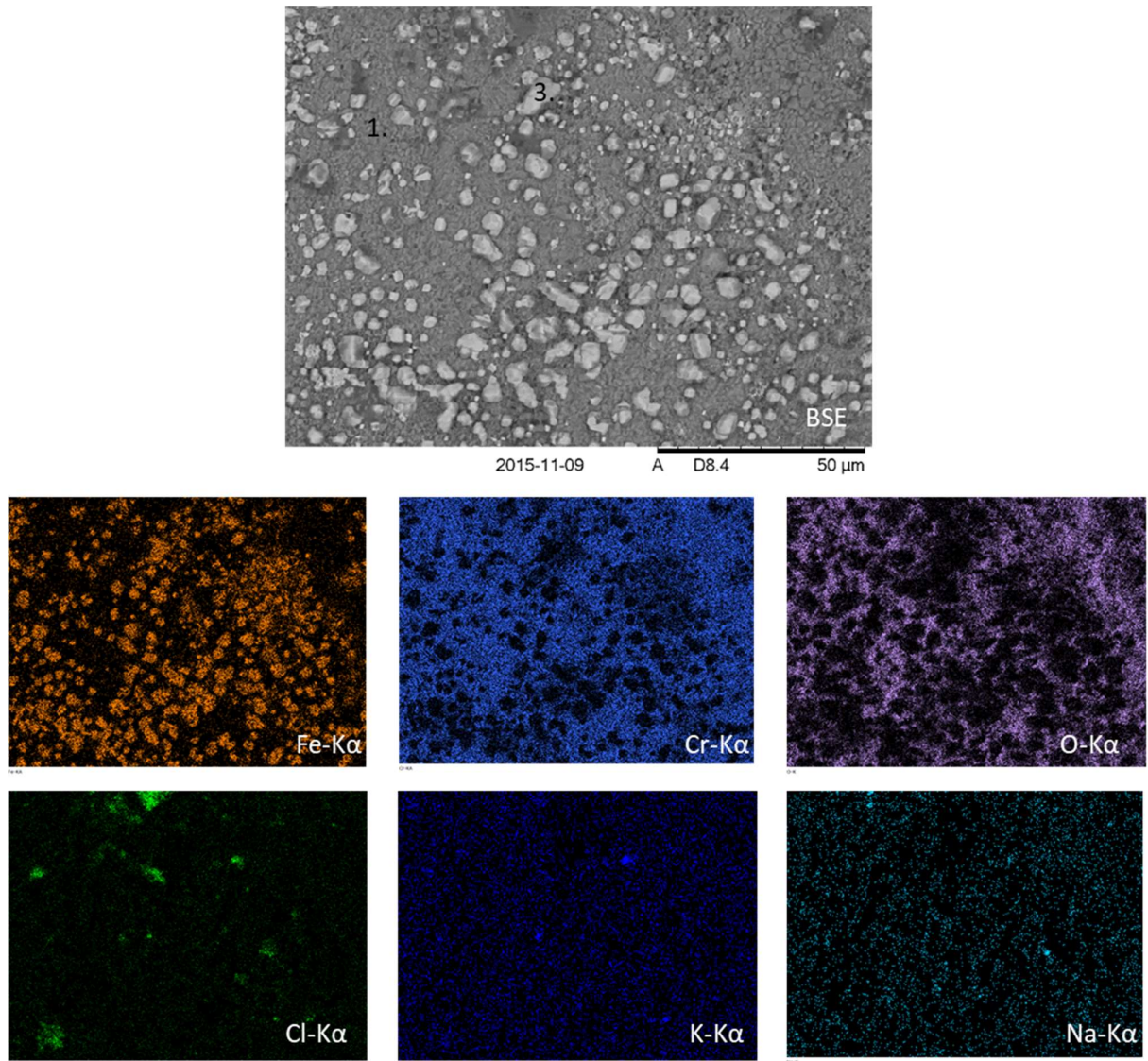
Figure 4.6: BSE image and corresponding EDX elemental maps for the surface of a stainless steel 316L coupon immersed in a ternary molten alkali chloride eutectic for four weeks. Regions 1 and 4 are discussed in the text.

In addition to the EDX map in Figure 4.6, spot analysis has been conducted on region 1 in each image and the results (shown in Table 4.2) conclusively show that chromium and oxygen are present. Unfortunately, spot analysis on region 3 could not be completed as there were not enough EDX data points.

Table 4.2: Measured elemental composition (at. %) of the area marked as (1) in Figure 4.5.

Element	One week	Three weeks	Three weeks (repeat)	Four weeks
Chromium	57.56	58.05	56.10	46.56
Oxygen	38.19	41.95	37.64	45.27
Carbon	4.26		6.26	8.17

4.2.2: Binary Results

The results for the samples run in a binary salt (Figure 4.7) show a lot less consistency with respect to their crystal structure compared to the ternary samples. This contradicts the XRD results, which show relatively consistent results.

The one week test shows clear contrast between the bulk, 2 and the corrosion layer, 4, which is thick (the bulk cannot be observed beneath it), flat, and does not cover the full sample. There is substantial damage to the bulk in this sample, and the grain boundaries are clearly visible, suggesting that the corrosion product has not acted as a protective barrier as it does in the ternary tests (Figure 4.5). This has led to chloride acting as a fluxing agent and increasing the corrosion rate. This has been reported by several sources in the literature [12-14]. It also appears that the layer is made up of small blocky crystal structures, similar to those observed in Chapter 3 (Figure 3.17). It should be noted that this result was observed when the sample was immersed in a binary test, whereas the three week tests were conducted in a ternary salt.

Similar to the initial three week stainless steel 316L test in Chapter 3, the products of the three week binary tests, labelled 5 in Figure 4.7 are highly textured and difficult to analyse, but information about the shape of the corrosion product can be obtained. The BSE image (Figure 4.7) shows that the corrosion product consists of long thin closely packed crystals, believed to be tabular in crystal habit. This has not previously been seen. Results in Chapter 3 gave a blocky structure or a relatively flat layer formed on the surface. Additionally, this has not previously been reported in any of the literature. However, stainless steel 316L samples obtained by Sellers et al. [4] after a furnace failure, show similar visual results to the three week tests but the SEM images are not clearer meaning it is possible that this crystal structure has been formed on the surface of the sample in Sellers' work, but the unclear SEM images make it difficult to conclude [4].

The repeated three week test shows evidence of pitting on the bulk steel labelled as 2. The corrosion product 6 shows a similar blocky crystal to the stainless steel 316L three week test seen in Chapter 3 (Figure 3.17), and also the one week binary test. A further corrosion product 7 observed in this sample appears to have a massive or druzy structure.

The four week binary test shows similar results to those previously observed in this work. Two different and distinct corrosion products have formed (4 and 6) and they do not fully cover the sample. It appears that both of the corrosion products have previously been formed within this work, with the blocky structure forming in both three week stainless steel sample (Figure 3.17) and the more planar corrosion product 4 also being observed in the binary one week test.
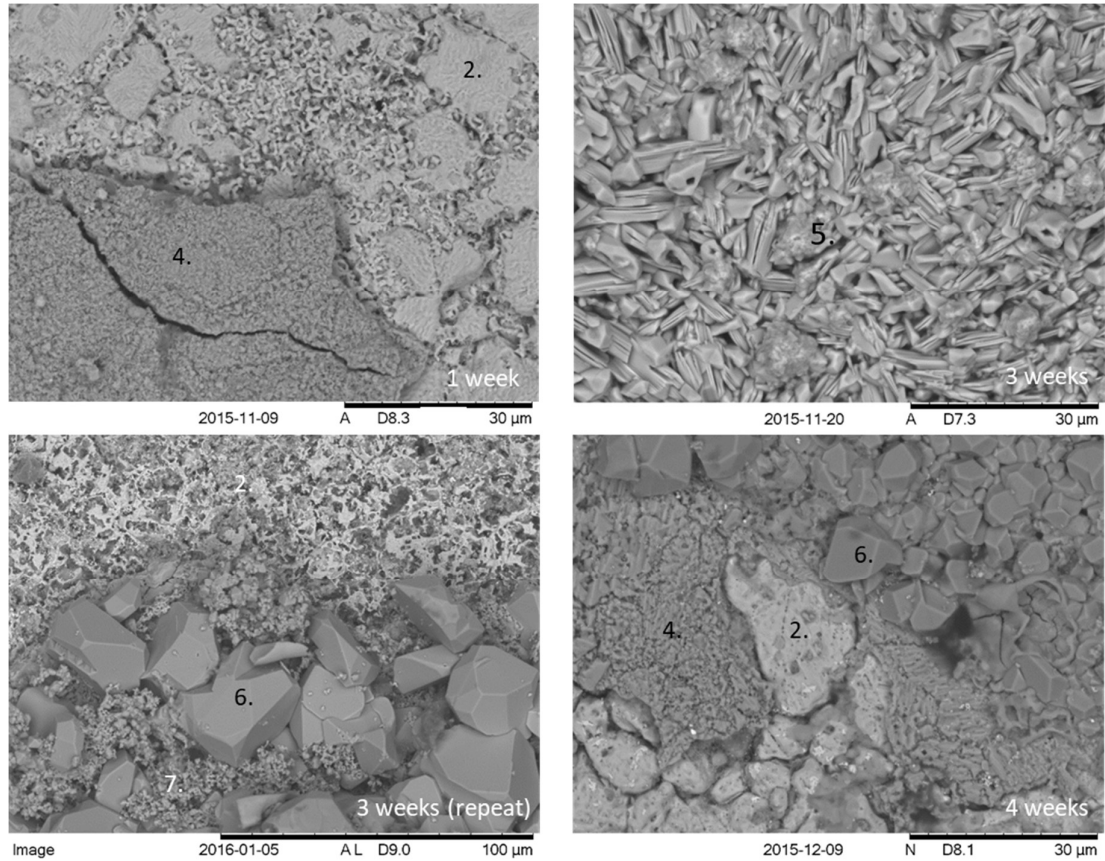
Figure 4.7: BSE images of stainless steel 316L held in a binary molten alkali chloride bath for a predetermined length of time (stated at the bottom of each image).

As numerous different corrosion products have been formed, EDX data for each of the samples will be presented.

The EDX analysis for a sample immersed for one week is shown in Figure 4.8, and it is clear that chromium and oxygen are present within the corrosion layer. It was first postulated that the three week tests in Chapter 3 showcased anomalous results, but the results obtained here show a similar 'blocky' crystal structure, although it is considerably smaller.
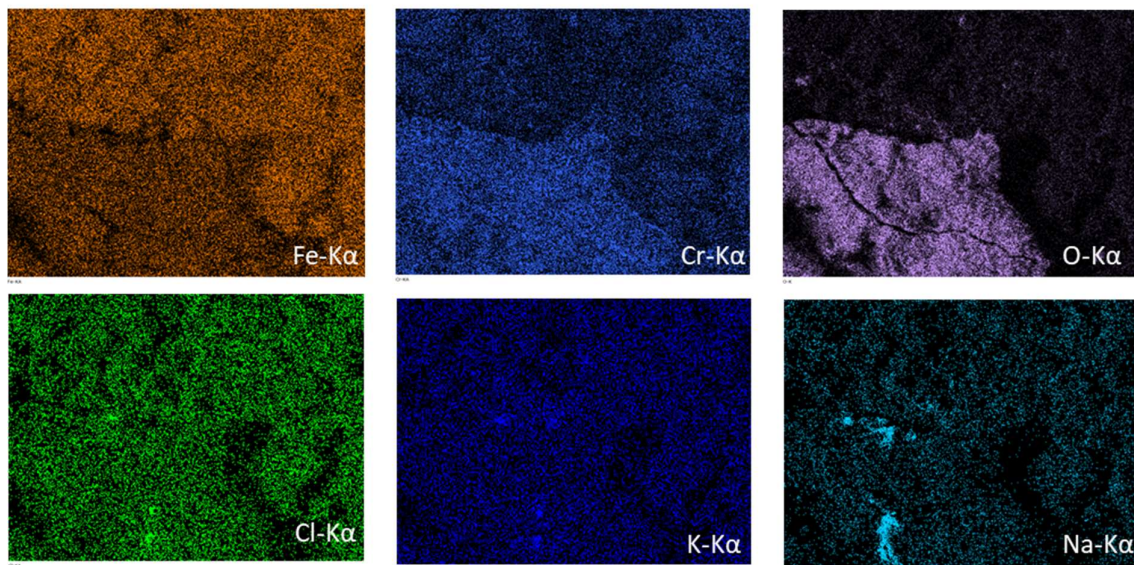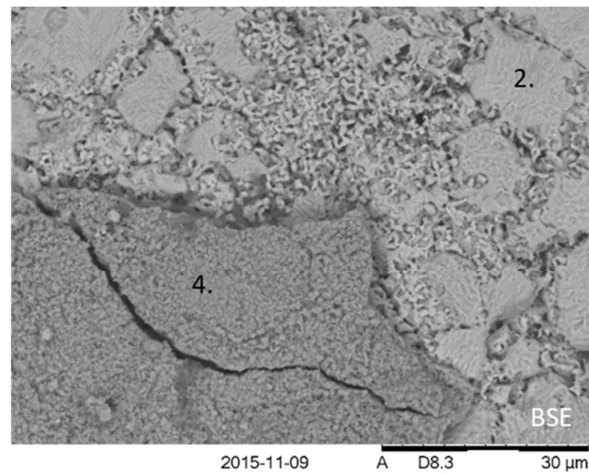
Figure 4.8: BSE image and corresponding EDX elemental maps for the surface of a stainless steel 316L coupon immersed in a binary molten alkali chloride eutectic for one weeks. Regions 2 and 4 are discussed in the text.

The surface SEM/EDX images for the initial three week binary test (Figure 4.9) show little contrast, and it should be noted that areas which appear to have no X-ray signal and appear to show a lack of a certain element actually correspond to areas which lack collected X-ray data. This has resulted in data that show little contrast, and it is therefore difficult to distinguish elements that are present. Figure 4.9 implies that the corrosion layer is made up of sodium, iron and oxygen. The chloride that would usually be associated with sodium is not observed, but it is possible that due to the porous nature of the corrosion product salt has become trapped within the layer. Shankar and Mudali [8] found that tests on stainless steel 316L in LiCl-KCl at 873K resulted in a porous corrosion product rich in chromium forming on the surface, and the morphology of the corrosion product changing as immersion time increases [8].
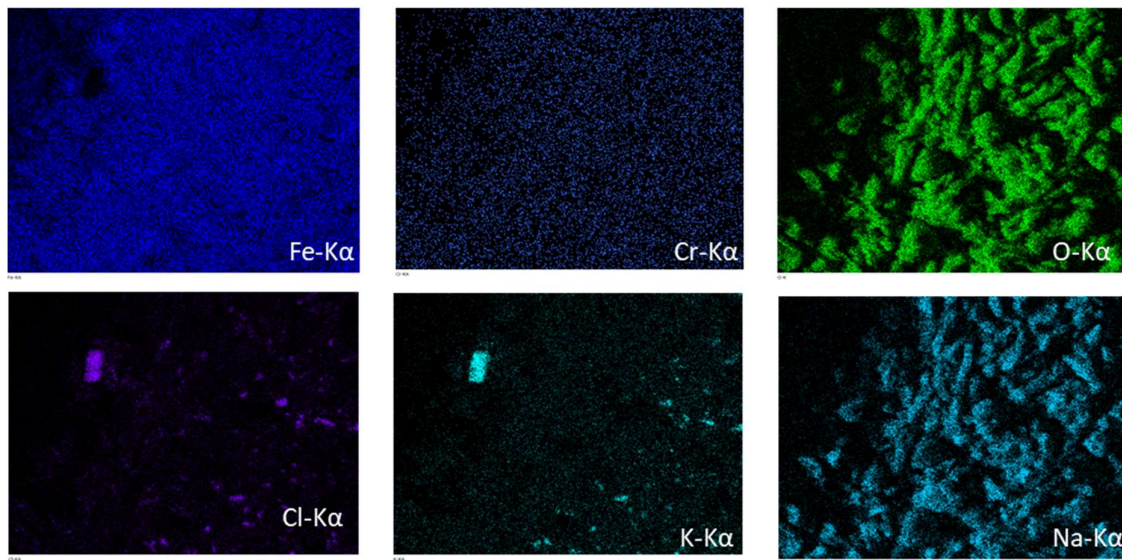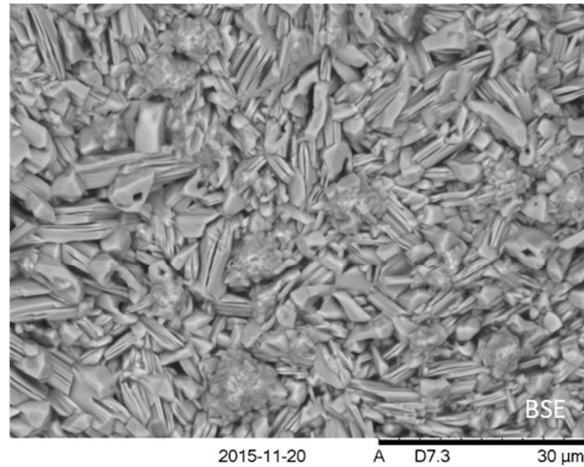
Figure 4.9: BSE image and corresponding EDX elemental maps for the surface of a stainless steel 316L coupon immersed in a binary molten alkali chloride eutectic for three weeks.

Figure 4.10 shows the surface SEM/EDX analysis for the repeated three week binary test. The images show that the corrosion product 6, which as previously mentioned is blocky in nature, is made up of chromium and oxygen, and it is also clear that a full corrosion layer has not been formed over the sample as the bulk, labelled 2 is still observable. There is also a further corrosion product 7, which has a massive or druzy structure and its elemental composition appears to consist of iron, chromium and oxygen. The results obtained can be related back to the results observed in Chapter 3, where the three week test showed the formation of numerous different iron oxides and chlorides and the four week test reverted back to the initially observed corrosion product, this has not been reported in any of the literature.
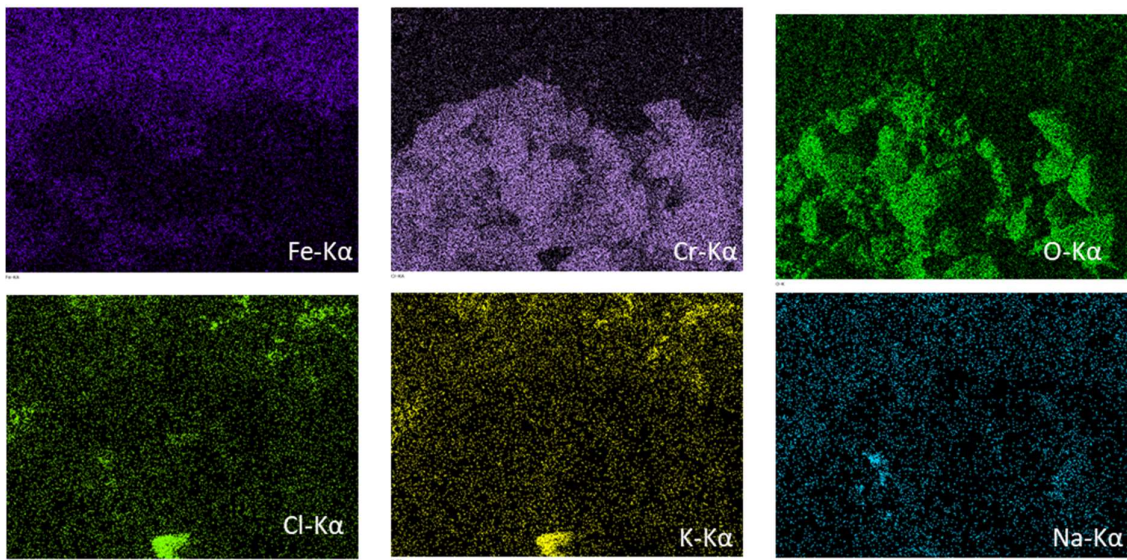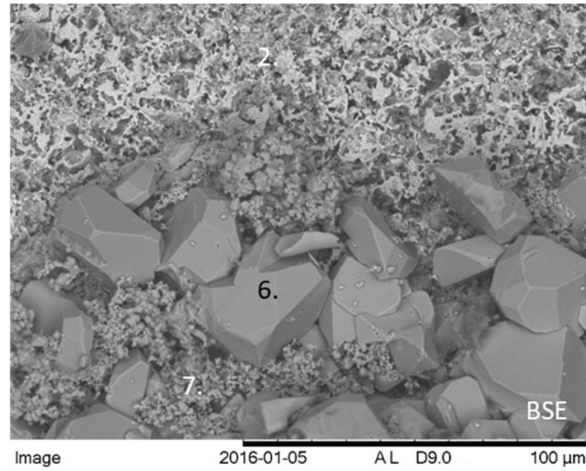
Figure 4.10: BSE image and corresponding EDX elemental maps for the surface of a stainless steel 316L coupon immersed in a molten binary alkali chloride eutectic for three weeks. Regions 2, 6 and 7 are discussed in the text.

Finally, the EDX data for the binary four week test are shown in Figure 4.11. Contrast is observed between the bulk 2 and the blocky structure 6, which is made up of chromium and oxygen. This is comparable to previous results In Chapter 3 (Figure 3.17) and also reiterates the results of the three week (repeated) binary tests (Figure 4.10). Figure 4.11 showcases a further corrosion product 4, which is made up of chromium and iron oxides, and appears to consist of small crystals penetrating into the stainless steel structure, similar to those seen in the one week binary tests (Figure 4.8).
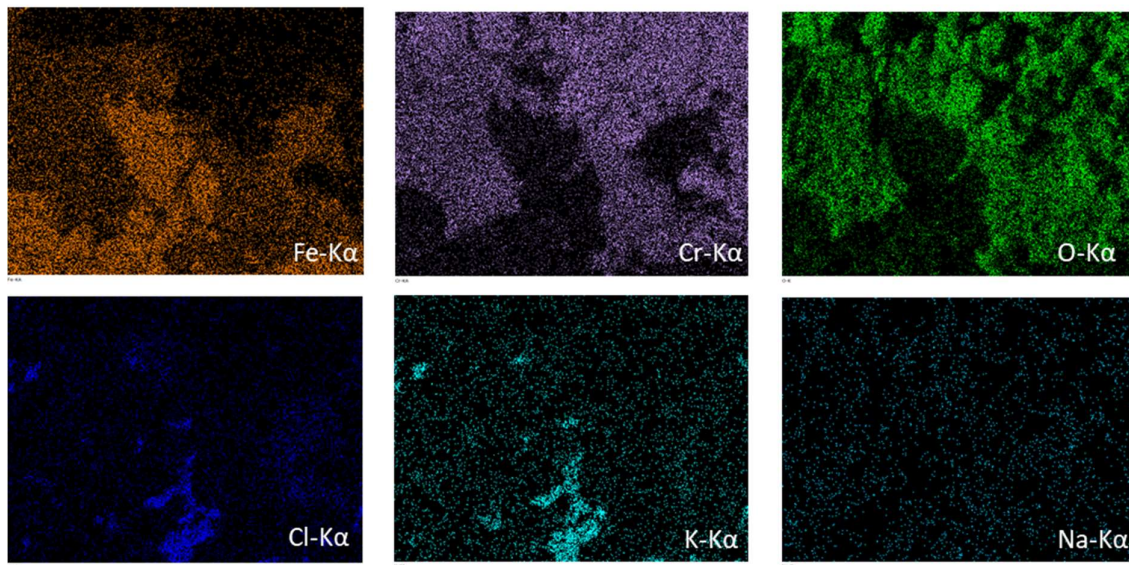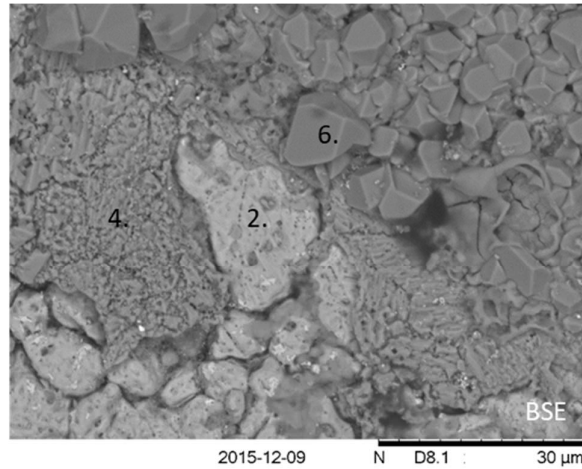
Figure 4.11: BSE image and corresponding EDX elemental maps for the surface of a stainless steel 316L coupon immersed in a molten binary alkali chloride eutectic for four weeks. Regions 2, 4 and 6 are discussed in the text.

In addition to the EDX maps in Figure 4.8-Figure 4.11, further spot analysis has been conducted on regions 4, 5, 6 and 7 in each image in which they appear, and the results are shown in Table 4.3. Although inconsistent results have been seen throughout the binary tests, the spot analysis is relatively consistent with the majority of corrosion products (4, 6 and 7) being made up of chromium and oxygen. The results for region 5, which was difficult to analyse due to the highly textured nature of the corrosion product, does correlate with the results obtained in Figure 4.9, but chlorine is not seen as prominently in the spot analysis, and this suggests that chlorine is only present as a salt.

Table 4.3: Measured elemental compositions of the corrosion products formed in the binary eutectic tests, Figure 4.8-Figure 4.11.

Element	One week - region 4	Four weeks - region 4	Three weeks - region 5	Three weeks (repeat) - region 7	Three weeks (repeat) - region 6	Four weeks - region 6
Chromium	63.68	40.46		43.66	60.17	57.63
Oxygen	29.06	29.84	17.64	24.95	30.04	29.67
Carbon	7.26	7.34	16.20	30.02	3.52	9.98
Iron		22.36	51.68		4.93	2.52
Sodium			14.48			0.20
Potassium				0.64	0.68	
Chlorine				0.73	0.66	

4.3: Cross Sectional Analysis

4.3.1: Ternary Results

The cross sectional analysis of the ternary samples is shown in Figure 4.12, and the results show that in the one and three week (repeat) tests, the corrosion layer is predominantly present on the surface of the bulk. The three and four week tests show that a corrosion product has penetrated into the bulk, this reiterates the results found in the surface SEM, where a corrosion layer has formed and a further corrosion product appears to be diffusing into the bulk. The EDX analysis for the four week test is shown in Figure 4.13, which allows both the corrosion products (1 and 3) to be analysed.
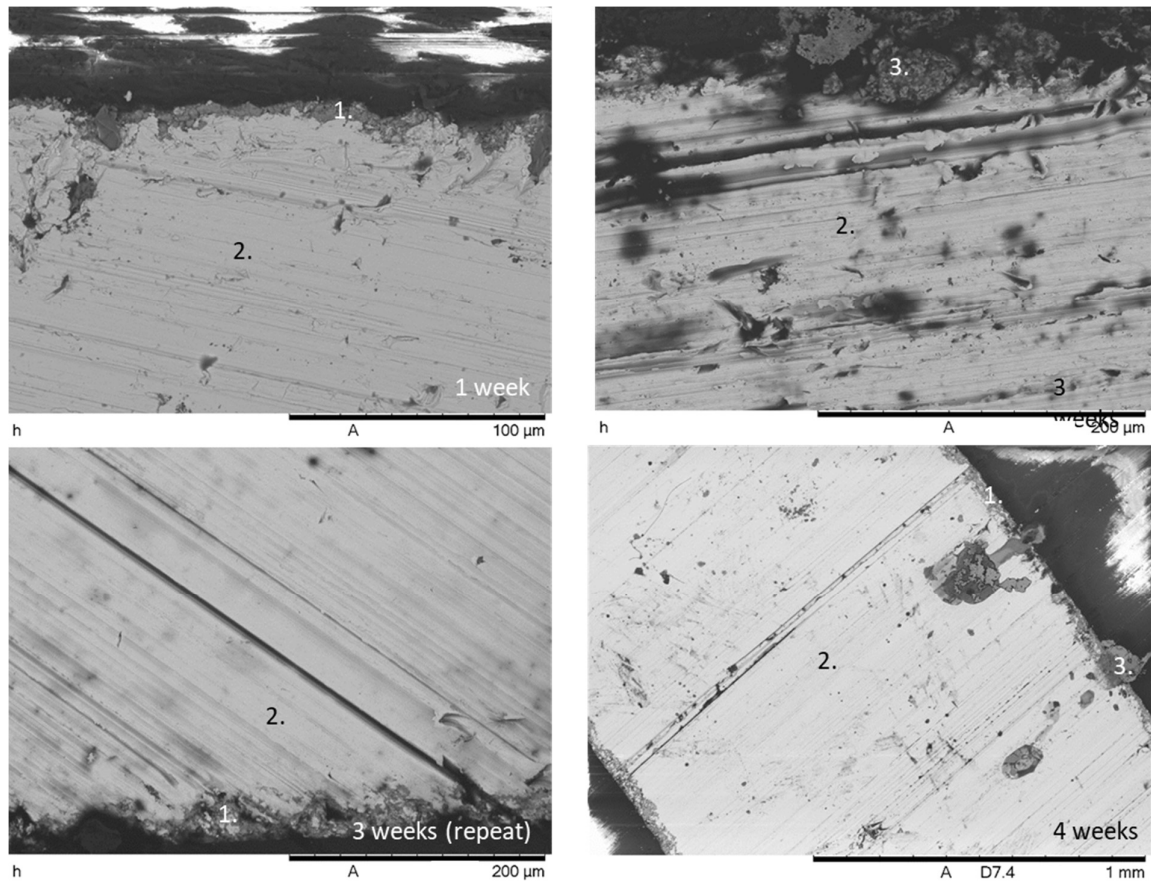
Figure 4.12: Cross-section BSE images of stainless steel 316L held in a ternary molten alkali chloride salt for a predetermined length of time (stated in the bottom right of each image).

The cross sectional EDX data shown in Figure 4.13 give information on the surface corrosion layer, which is made up of chromium and oxygen, and is present on all four of the ternary samples. As previously mentioned lithium cannot be detected by the instrument used in this work, but from the XRD analysis it is assumed that lithium chromium oxide is present. Further analysis into the crystal structures found in the surface EDX analysis shows that corrosion product 3 has penetrated the bulk. It is not conclusive, but it appears oxygen is present in corrosion product 3 although the oxidised metal is difficult to pinpoint in this analysis. Combining the information from the surface and cross sectional SEM/EDX, it is likely that iron oxide is present.
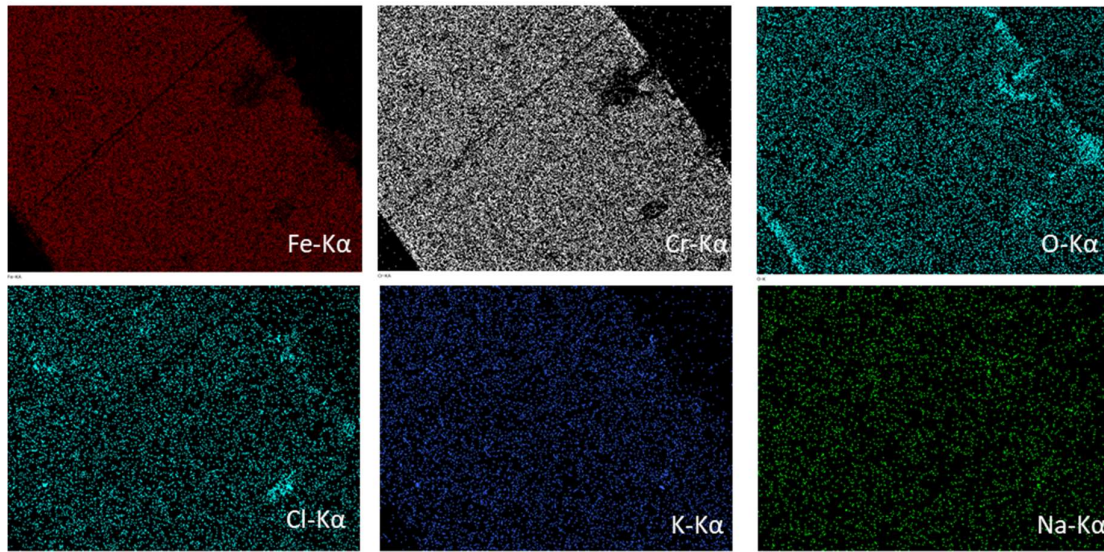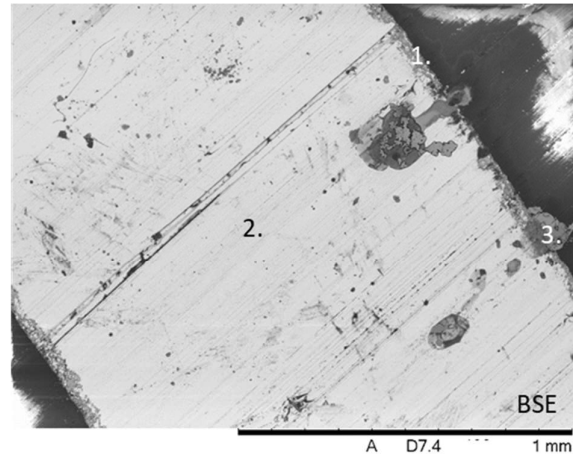
Figure 4.13: Cross-sectional BSE image and corresponding EDX elemental maps of the stainless steel 316L coupon immersed in a ternary molten alkali chloride salt for four weeks. Regions (1) and (3) are discussed in the text.

4.3.2 Binary results

The BSE cross sectional results can be seen in Figure 4.14, where the corrosion layer in the one week tests seems to have penetrated further into the bulk (approx. 10 μm) compared to the ternary results (approx. 1 μm) (Figure 4. 12). Due to the lack of lithium chloride this was expected. Similar results are also obtained in the three week repeat test, with a higher level of attack compared to the one week tests due to the increased immersion time. The initial three week test shows large voids (the largest being approximately 0.5 mm) between the corrosion layer and the sample. This has not been seen in Chapter 3 but has been reported in the literature by Shankar and Mudali [8] and also by Sellers et al. [4]. Finally, the four week test shows the presence of a corrosion product that sporadically appears

along the length of the surface. It is thick and extends further into the bulk compared to previously identified corrosion products.
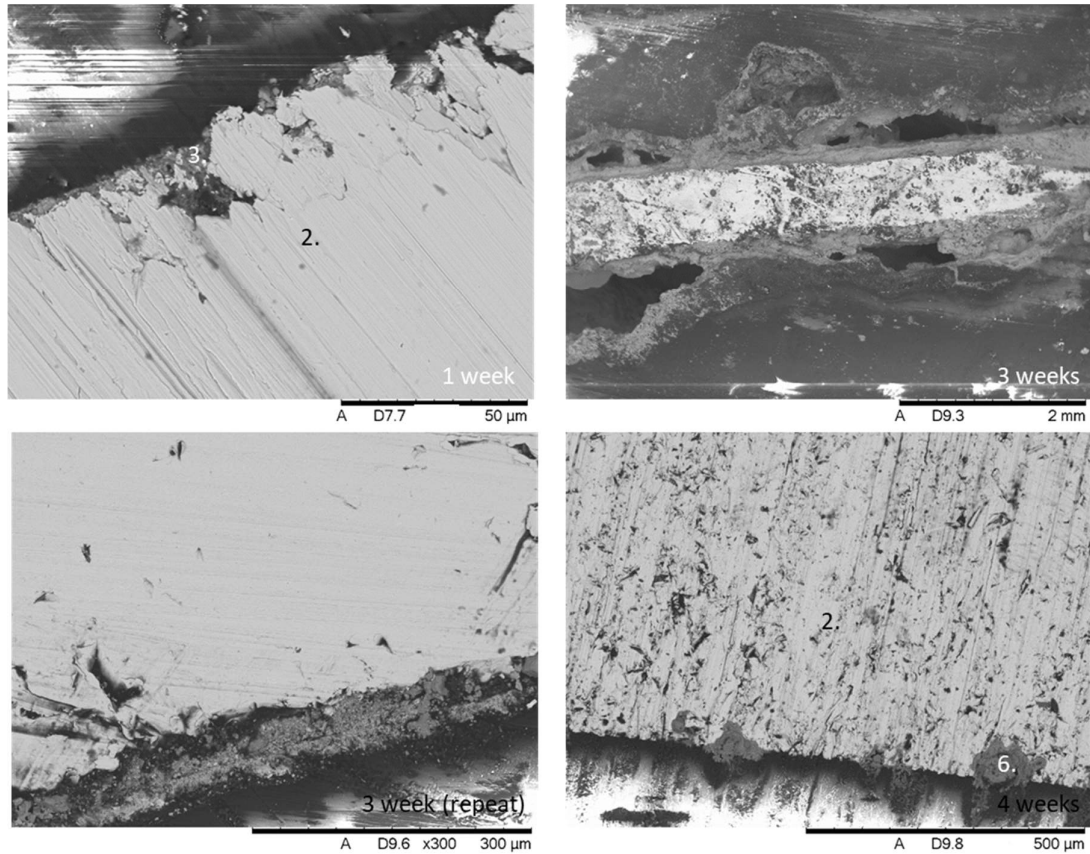
Figure 4.14: Cross-section BSE images of stainless steel 316L held in a binary molten alkali chloride salt for a predetermined length of time (stated in the bottom right of each image).

The EDX data are shown for the three week sample (Figure 4.15) along with the three week repeat (Figure 4.16) and the four week sample (Figure 4.17), all of which show slightly different results.

The cross section analysis for the three week test (Figure 4.15) shows oxygen along the corrosion layer surrounding the void and also within the corrosion layer formed on the surface. Sodium can also be seen, and it appears iron is the main metal present. This reiterates the observations in the surface SEM/EDX (Figure 4.9). Sodium is also observed in conjunction with chlorine, implying that some salt is trapped within the layers. It is postulated that the voids formed are due to the sublimation of iron (II) chloride at 700°C [15]. This was also seen in Sellers et al's. work [4].

Figure 4.16 shows the cross sectional images obtained for the repeated binary three week sample and it is evident that salt is trapped within a chromium, iron and oxygen corrosion layer. It is difficult to state that iron is present in the surface images as it will always be detected due to the bulk, but it is clearly present in the cross sectional analysis.

The EDX analysis shown in Figure 4.17 suggests that region 6 is made up of iron and oxygen. This contradicts what has been observed in the surface SEM/EDX, Figure 4.11, where a chromium oxide corrosion product appeared to have been formed via attack of the stainless steel bulk. It is therefore suggested that it is possible that an iron based compound has also formed on the surface.
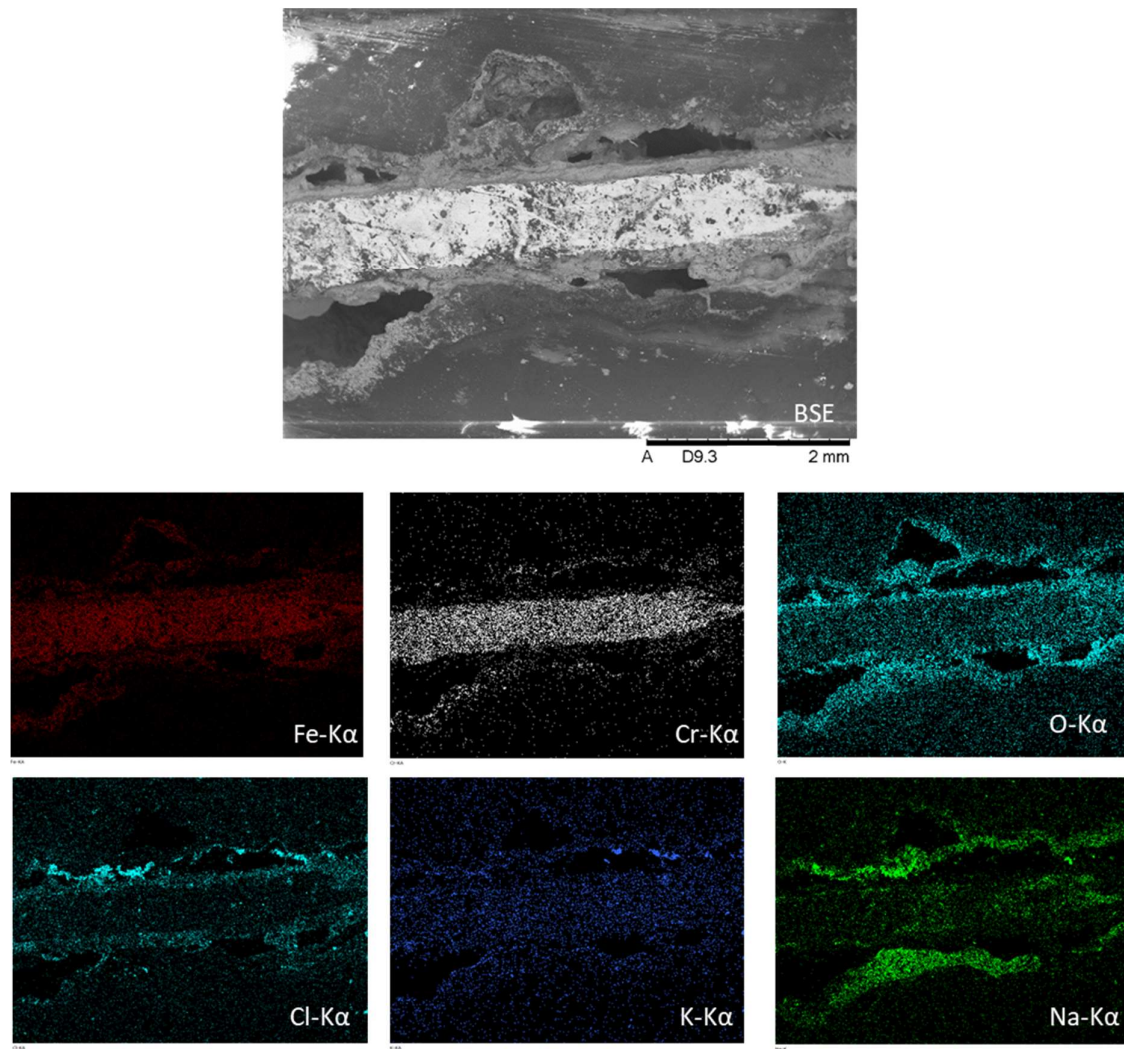
Figure 4.15: cross-sectional BSE image and corresponding EDX elemental maps of the stainless steel 316L coupon immersed in a binary molten alkali chloride salt for three weeks.
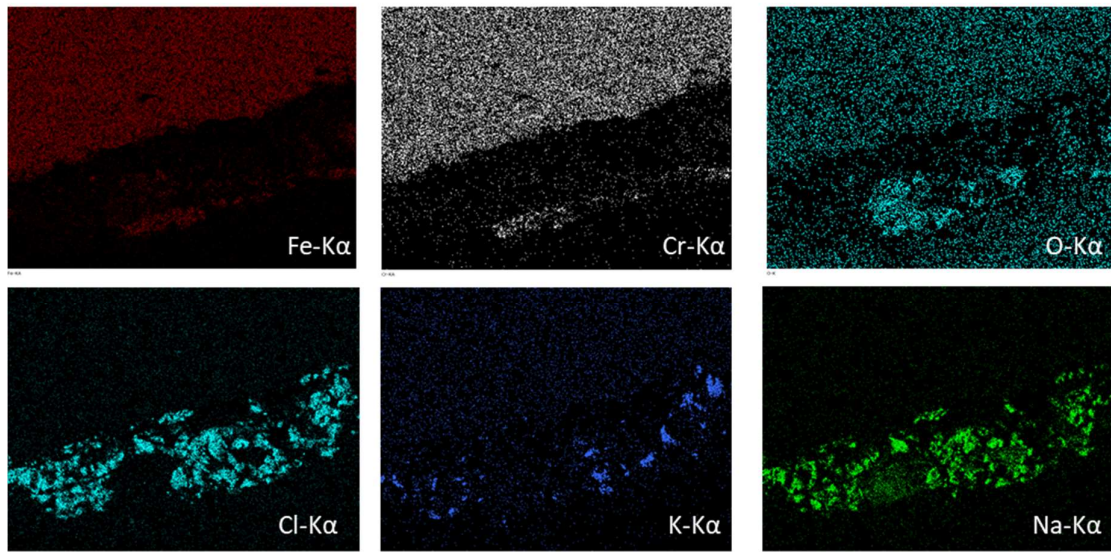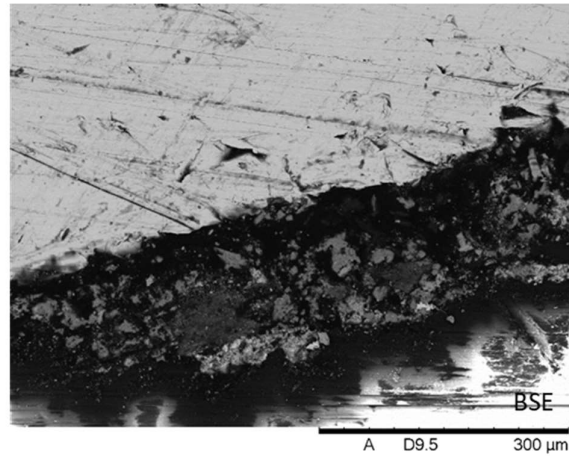
Figure 4.16: Cross-sectional BSE image and corresponding EDX elemental maps of the stainless steel 316L coupon immersed in a binary molten alkali chloride salt for three weeks.
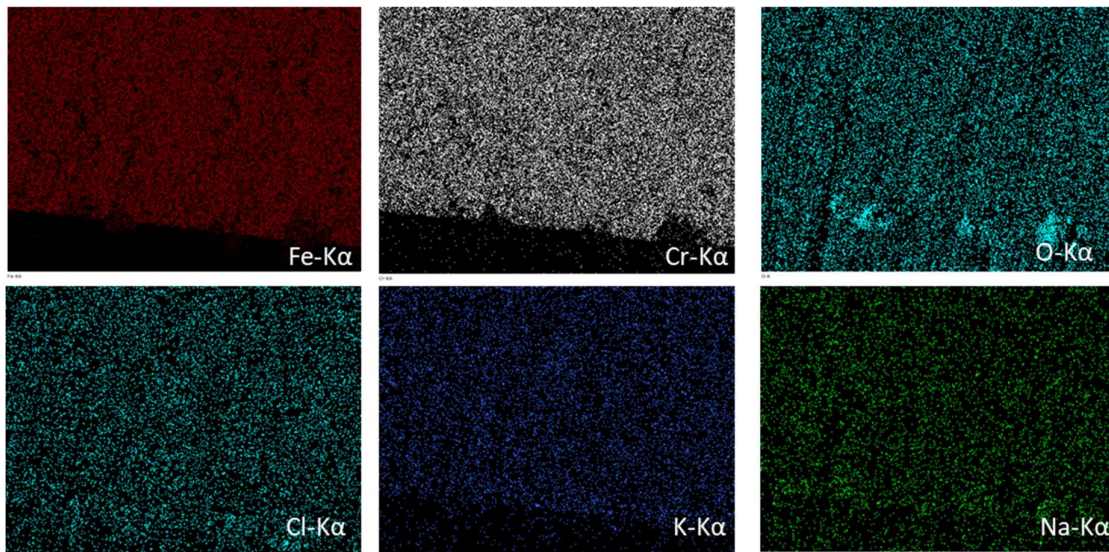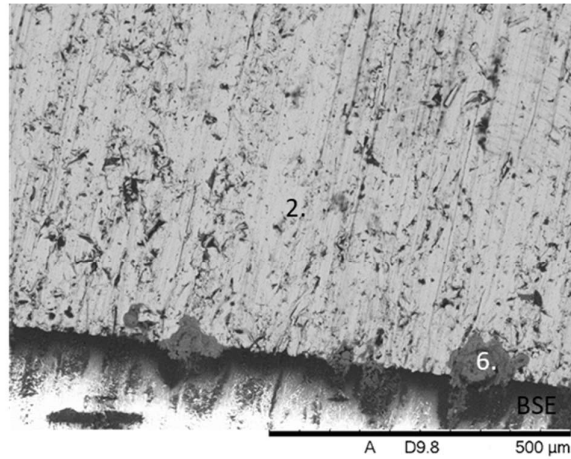
Figure 4.17: Cross-sectional BSE image and corresponding EDX elemental maps of the stainless steel 316L coupon immersed in a ternary molten alkali chloride salt for four weeks. Region (6) is discussed in the text.

4.3 Conclusions

This chapter aimed to investigate the role of lithium within the formation of the corrosion product. It is clear that lithium is essential for the formation of a corrosion layer that covers the majority of the stainless steel surface. The tests show that a protective layer has formed over the ternary sample and the EDX data suggest that the elements present in the layer are chromium and oxygen.

The ternary eutectic experiments showed consistent results throughout this work, with the formation of a uniform lithium chromium oxide layer. The binary tests showed the corrosion of stainless steel when lithium is not present.

The binary results are a little less predictable. The one week test shows the presence of a corrosion layer, thicker than that observed for the ternary samples, which does not cover the full sample. The major elements present in this layer are chromium and oxygen. The structure of the corrosion product

is also different from previously observed layers, as the corrosion layer is made up of small tightly packed crystals. Similar results are observed for the repeated three week tests and the four week tests, with the formation of a blocky compound on the surface of the sample. The four week test also shows the formation of a corrosion product that penetrates the bulk and it appears to be made up of iron and oxygen, this was not observed in the surface analysis, but it is possible that this particular corrosion product was not imaged.

The obvious anomalous result in this work is seen at three weeks, and although this does not follow the pattern of other binary samples, odd results have previously been seen at three weeks in Chapter 3. The initial three week tests show the formation of a thick porous corrosion layer with voids formed between the corrosion layer and the bulk and it is likely that a different corrosion route has been taken compared to other samples. It should also be noted the layer formed over the surface is easily removed and sporadic.

The SEM/EDX data clearly show that at least two different corrosion paths have been taken in this work, and that the presence of lithium is essential, if a protective layer to protect against molten chloride is required.

The role of chromium has proven to be essential in the formation of a corrosion layer, therefore the next chapter will investigate the role of stainless steel composition on corrosion in a ternary molten salt.

Literature cited

1. S. Frangini, A. Masci, and F. Zaza, *Molten salt synthesis of perovskite conversion coatings: A novel approach for corrosion protection of stainless steels in molten carbonate fuel cells.* Corrosion Science, 2011. **53**(8): p. 2539-2548.
2. D.S. Coleman and P.D.A. Lacy, *The phase equilibrium diagram for the KCl-NaCl system.* Materials Research Bulletin, 1967. **2**(10): p. 935-938.
3. R.A. Guidotti and P.J. Masset, *Primary Batteries – Reserve Systems | Thermally Activated Batteries: Lithium*, in *Encyclopedia of Electrochemical Power Sources*, J. Garche, Editor. 2009, Elsevier: Amsterdam. p. 141-155.
4. R.S. Sellers, M.H. Anderson, K. Sridharan, and T.R. Allen, *Failure analysis of 316L stainless steel crucible by molten fluoride salt interaction with clay bonded silicon carbide.* Engineering Failure Analysis, 2014. **42**: p. 38-44.
5. S.-H. Cho, J.-M. Hur, C.-S. Seo, and S.-W. Park, *High temperature corrosion of superalloys in a molten salt under an oxidizing atmosphere.* Journal of Alloys and Compounds, 2008. **452**(1): p. 11-15.
6. N. Hiramatsu, Y. Uematsu, T. Tanaka, and M. Kinugasa, *Effects of alloying elements on NaCl-induced hot corrosion of stainless steels.* Materials Science and Engineering: A, 1989. **120**: p. 319-328.
7. H.E. McCoy, *Status of Materials Development for Molten Salt Reactors*. 1978, Oak Ridge National Laboratory
8. A.R. Shankar and U.K. Mudali, *Corrosion of type 316L stainless steel in molten LiCl–KCl salt.* Materials and Corrosion, 2008. **59**(11): p. 878-882.

9.   L.C. Olson, *Materials Corrosion in Molten LiF-NaF-KF Eutectic Salt*, in *Department of Engineering Physics*. 2009, University of Wisconsin-Madison.

10.   H.S. Khatak and B. Raj, *Corrosion of Austenitic Stainless Steels Mechanism, Mitigation and Monitoring.* 2002, Woodhead: Cambridge.

11.   P. Biedenkopf, M. Spiegel, and H.J. Grabke, *High temperature corrosion of low and high alloy steels under molten carbonate fuel cell conditions.* Materials and Corrosion, 1997. **48**(8): p. 477-488.

12.   W.D. Manly, J. G. M. Adamson, J.H. Coobs, J.H. DeVan, D.A. Douglas, E.E. Hoffman, and P. Patriarca, *Airraft Reactor Experiment- Metallurgical Aspects*. 1957, Oak Ridge National Laboratory.

13.   K. Sridharan and T.R. Allen, *Corrosion in Molten Salts* in *Molten Salts Chemistry*, H. Groult and F. Lantelme, Editors. 2013, Elsevier: Oxford. p. 241-267.

14.   A. Nishikata, H. Numata, and T. Tsuru, *Electrochemistry of molten salt corrosion.* Materials Science and Engineering: A, 1991. **146**(1): p. 15-31.

15.   D.L. Perry, *Handbook of Inorganic Compounds*. 2011: CRC Press. Taylor and Francis Group